analytical chemistry

Article

Cite This: *Anal. Chem.* 2019, 91, 9058−9068

pubs.acs.org/ac

Enhanced Ion Yields Using High Energy Water Cluster Beams for Secondary Ion Mass Spectrometry Analysis and Imaging

Sadia Sheraz,[†] Hua Tian,[*,‡] John C. Vickerman,[†,§] Paul Blenkinsopp,[¶] Nicholas Winograd,[‡] and Peter Cumpson[†]

[†]School of Mechanical and Systems Engineering, University of Newcastle, Newcastle NE1 7RU, United Kingdom

[‡]Department of Chemistry, Pennsylvania State University, State College, Pennsylvania 16802, United States

[§]Manchester Institute of Biotechnology, University of Manchester, Manchester M1 7DN, United Kingdom

[¶]Ionoptika Ltd, Chandlers Ford SO53 4BZ, United Kingdom

Supporting Information

ABSTRACT: Previous studies have shown that the use of a 20 keV water cluster beam as a primary beam for the analysis of organic and bio-organic systems resulted in a 10−100 times increase in positive molecular ion yield for a range of typical analytes compared to C_{60} and argon cluster beams. This resulted in increased sensitivity to important lipid molecules in the bioimaging of rat brain. Building on these studies, the present work compares 40 and 70 keV water cluster beams with cluster beams composed of pure argon, argon and 10%CO_2, and pure CO_2. First, as previously, we show that for E/nucleon about 0.3 eV/nucleon water and nonwater containing cluster beams generate very similar ion yields, but below this value, the water beams yields of BOTH negative and positive "molecular" ions increase, in many cases reaching a maximum in the <0.2 region, with yield increases of ∼10−100. Ion fragment yields in general decrease quite dramatically in this region. Second, for water cluster beams at a constant E/nucleon, "molecular" ion yield increases with beam energy and hence cluster size due to increased sputter yield (ionization probability is constant). Third, as a consequence of the increased ion yield and the improved focusability using high-energy cluster beams, imaging in the 1 μm spatial resolution region is demonstrated on HeLa cells and rat brain tissue, monitoring molecules that were previously difficult to detect with other primary beams. Finally, the suggestion that the secondary ion emission zone has quasi-aqueous character seems to be sustained.

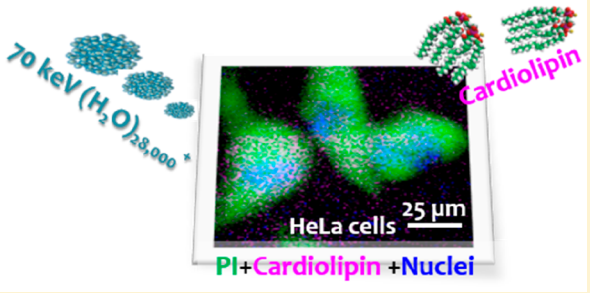

As many papers on this topic commence, "ToF-SIMS is now widely accepted as a useful analytical technique for spatially resolved chemical analysis of a wide range of materials, especially of a biological nature."[1−5] ToF-SIMS complements imaging MALDI and DESI by providing a greater potential for submicrometer resolution.[6] The advent of GCIB beams using argon and CO_2 clusters has resulted in very gentle ion emission and hence almost zero chemical damage to the analyte and very low fragmentation of the emitted "molecular" ions.[7−12] The ability to depth profile through complex molecular systems with good depth resolution is a powerful capability that provides unique information.

Although the capabilities of ToF-SIMS are considerable, the yield of detectable ions is not high and is influenced by the chemical environment in the emission zone, the so-called matrix effect. As a consequence, although sophisticated ion beam systems have been developed that in principle enable submicrometer resolution, in some cases down to or below 100 nm, the yield of ions from these very small emission areas is so small that useful numbers of ions for analysis are impossible to obtain.[13] Thus, the number of ions that can be detected frequently limits the useful spatial resolution. Furthermore, the relative yields of ions originating from different components in the analyte will be influenced not only by their concentration, but as a consequence of the matrix effect also by the chemistry of the analyte, thus without careful calibration there may not be a direct relationship between signal intensity and sample composition.[14−16]

Generally, it seems that the *Useful Yield* (UY) of secondary ions in organic systems is at best around 10^{-5} (this is a measure of the number of ions counted by the detection system compared to the number of related molecules removed in the sputtering process).[17−20] As a result, the average number of molecular ions obtained from a 1 μm^2 pixel area is less than 0.01 under static conditions (<1% of surface removed). Whether a sputtered species is detected as an ion is dependent on the ionization probability of the species (molecule), the degree to which it is fragmented as a consequence of emission and ionization and the efficiency of the ion transmission and detection of the spectrometer. Recent studies by Wucher et al.

Received: March 18, 2019
Accepted: May 23, 2019
Published: May 28, 2019

DOI: 10.1021/acs.analchem.9b01390
Anal. Chem. 2019, 91, 9058−9068

have shown that the positive ionization probability of several different organic molecules lies close to 10^{-3}.[21] This suggests that ion fragmentation and instrument transmission are responsible for the other losses. The use of large primary cluster ions should result in low impact energies per cluster component that reduces the potential for sputter induced fragmentation of the emitted secondary ion.[22,23] Ion transmission efficiency is a function of the mass spectrometer design and complexity. It is speculated that to account for the low reported useful yields of 10^{-6}−10^{-5}, the efficiency cannot be more than about 10^{-1}, the improvement of which will have to rely on the instrument manufacturers.

From the above analysis, it can be seen that if we are to improve the *Useful Yield* to enable informative analysis at the submicrometer level, some improvement in ionization probability and ion transmission together with a lowering of ion fragmentation is required. Ion fragmentation is an outcome of the ion formation process and other than lowering the energy input during sputtering, it is not clear that anything dramatic can be done, except perhaps introducing some sort of ion cooling process. Ion transmission is perhaps something that ToF-SIMS instrument manufacturers could look at with some benefit. At present, ionization probability is the source of most of the loss of ion yield so it has attracted most experimental activity with a view to increasing yields. A number of groups have investigated the possibility of enhancing the secondary ion yields from organic and bio-organic analytes by adding compounds or metals to the surface.[24−28] These methods are usually system specific, and the addition of further chemistry to what are frequently quite complex materials is not always to be recommended. Additionally, they are not readily applicable in 3D analytical applications. So far, we have focused on the possibility of enhancing proton *positive* ion yield using water cluster beams.[29−31] The idea was based on the observations of a number of groups that the presence of water, either adventitious or intentionally added, promoted the yield of protonated molecules and related secondary ions.[32−34] As a consequence of our previous studies, it has been shown that there is a significant positive ion yield benefit to be obtained from the use of water clusters as primary ion beams in the analysis of bio-organic molecules. This benefit is particularly significant for ToF-SIMS if an instrument is used that can collect all the ions generated well beyond the static limit that previously constrained analysis using high energy small metal cluster primary ions.[35]

Argon cluster beams can be used as very effective primary beams for the analysis of biological systems, and it has been shown that they are optimally effective where the primary energy per argon atom, E/n, is below about 10 eV.[30] Although molecular fragmentation falls below this energy, yield does too. Recently, the use of cluster beams incorporating CO_2 have been increasingly advocated.[11,36,37] It seems that van der Waals forces between CO_2 molecules in the beam increase beam cohesion and hence focusability. There is also some evidence of increased ion yield in some cases.[38]

Water cluster beams seem to behave in a similar manner to argon at $E/n \geq 10$ eV; however, in contrast to the behavior observed using argon and CO_2 cluster beams, the yield of $[M + H]^+$ ions rises significantly to a maximum as E/n falls to around 2 eV or, equivalently, as the cluster size increases to ≥7000 at 20 keV beam energy.[30] The yield enhancement using water cluster beams varies with the chemistry of the analyte. In the cases studied to date, the increase for $(nM + H)^+$ ions is in the region of 10−100 times. There is also some evidence that the matrix effect is ameliorated.[39,29,40] Studies with $(D_2O)_n$ cluster beams have shown that enhanced protonation in the low E/n regime does arise principally from the water molecules in the cluster.[30] The mechanism of water cluster ion yield enhancement is a matter of some speculation; however, it is possible to derive some insights by combining molecular dynamics (MD) modeling with empirical considerations[41−44] and the observations from our experiments. On this basis, it is suggested that in the impact site some type of concerted mechanism occurs between the energized water cluster and the analyte molecules to enhance the protonation process. It seems that close to an aqueous environment is created in the emission zone, and this idea has been supported by recent studies showing that the yield using water beams is very similar to the yield using argon cluster beams from analyte in a frozen hydrated matrix.[39]

These studies suggested that using the water cluster beam may have enhanced the ionization probability of the molecules studied to 10^{-2} or above, a very encouraging result. A subsequent study applied 20 keV water cluster beams $(H_2O)_n$ and what was termed "wet" argon cluster beams (an argon cluster beam dosed with water at a partial pressure just below 1 bar) to imaging a mouse brain tissue.[40] Particular attention was given to the influence of the two types of beam on the yield of various tissue lipids. The 20 keV water-containing cluster beams where the beam energy per nucleon (E/nucleon) ≈ 0.2 eV were found to be optimum for enhancing ion yields dependent on protonation. Ion yield enhancements over those observed using Ar_{2000}^+ again lie in the range 10−100 using the $(H_2O)_{6000}^+$ beam, while with water-doped $(H_2O)Ar_{2000}^+$, they lie in the 4−10 range. Of particular interest was the observation that whereas using argon cluster beams, cholesterol is not observed in the gray matter regions of the brain, with the water containing beams, it is observed in both white and gray matter regions as would be expected.[40] Although the differing physical structures of white and gray matter probably play a role, it is clear that the well-known suppressing effect of phospholipids on the ionization of cholesterol is greatly reduced in gray matter in the presence of the water beams.

It seems that water beams could well become an important route to higher sensitivity imaging of biosystems with reduced matrix effect complications. There are, however, a number of interesting issues arising from the studies so far. First, what about the yield of negative ions that are an important source of data in SIMS imaging? For technical reasons, at the time we were not able to explore negative ion yields in our first studies. Second, there was evidence that ion yields at a given E/n rose with beam energy, in other words, with cluster size. This was demonstrated between 5 and 20 keV in our first paper. Is there a limit to this rise in yield with cluster size? Third, is it possible exploit the enhanced ion yields to push the useful spatial resolution attainable with a water cluster beam down to the 1 μm region? Finally, can we obtain a clearer idea as to the mechanism of ion formation that provides the yield enhancement? This article reports on studies that seek to provide insights into these issues using cluster beams in the energy region 40−70 keV.

Our studies have been carried out at Newcastle (UK) and Penn State Universities (USA) and will compare 40 and 70 keV water cluster beams with cluster beams composed of pure argon, argon and CO_2, and pure CO_2. There are two aims to

DOI: 10.1021/acs.analchem.9b01390
Anal. Chem. 2019, 91, 9058−9068

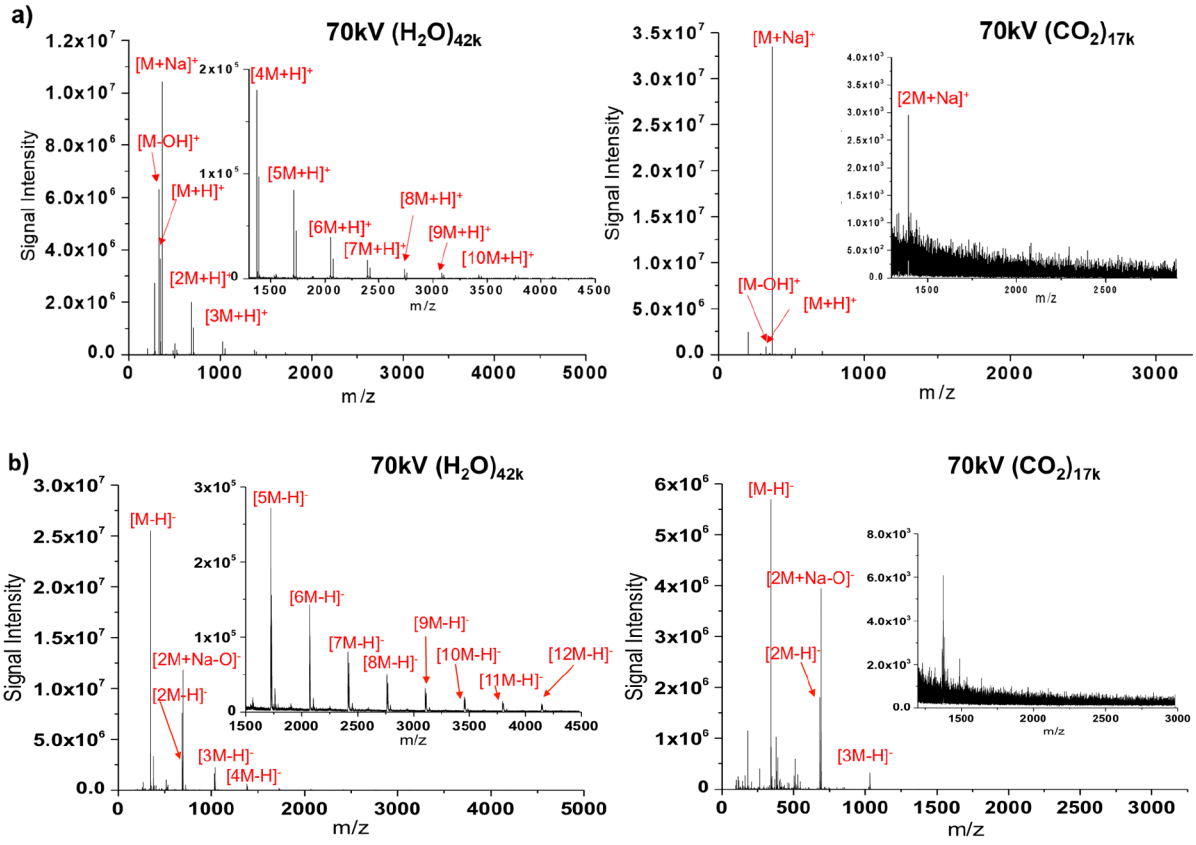

Figure 1. Positive (a) and negative (b) ion spectra from trehalose obtained using (a) 70 keV $(CO_2)_{17000}$ and (b) 70 keV $(H_2O)_{42000}$ cluster beams with a primary ion dose of 2×10^{12} ions cm^{-2} after sputtering to steady state.

this research. First, to explore further the degree to which water cluster beams may enhance positive *and negative* ion yield over that observed with argon or CO_2 cluster beams and to assess how increasing the beam energy influences the yield. Second, the research aims to explore the extent to which imaging of biomaterials benefits from the use of water cluster beams.

EXPERIMENTAL SECTION

Material and Sample Preparation. Ion yield studies were carried out on thin spin-cast films of four biorelated compounds: trehalose, a phosopholipid, 1-palmitoyl-2-oleoyl-*sn*-glycero-3-phosphocholine (POPC), [Asn[1] Val[5]] angiotensin II, and a cardiolipin (1,1′,2,2′ tetraoleoyl cardiolipin (sodium salt)). The preparation of the films is outlined in the Supporting Information.

TOF-SIMS Studies. TOF-SIMS analysis was performed on two J105 3D Chemical Imager instruments (Ionoptika Ltd., UK) described in detail previously.[35] One located at the University of Newcastle, UK is equipped with a 40 keV C_{60}^+ primary ion beam (Ionoptika Ltd., UK) and a 40 keV gas cluster ion beam (GCIB) system also supplied by Ionoptika Ltd, with a source that can provide either argon cluster or water cluster beams.[30] The second J105 instrument located at Pennsylvania State University, USA, is also equipped with an Ionoptika 40 keV C_{60}^+ primary ion beam, together with a new generation gas cluster ion beam, GCIB SM (Ionoptika, UK) that is designed to operate at high energies, up to ~70 keV, providing CO_2 or water cluster beams with a cluster size of up to several tens of thousands of molecules.[10] Our primary interest was to explore the E/nucleon region below 0.3, so this governed our choice of beam cluster size. The following ion beam configurations were used. At Newcastle 40 keV argon $(Ar)_n$ cluster beams where n varied from 3000 to 20000. Water cluster beams $(H_2O)_n$ where n varied from 8000 to 42000. At Penn State, $(CO_2)_n$ cluster beams are preferred to argon because they are easier to focus. Some small enhancement of yield is observed over argon for some samples. 70 keV $(CO_2)_n$ cluster beams were utilized with n varying from 3000 to 10000. The 70 keV $(H_2O)_n$ cluster beams with n in the range 13000 to 40000 were studied. Detail on the analysis and imaging procedures used are provided in the Supporting Information.

Cell and Tissue Imaging. To explore the benefits of enhanced ion yields under water beams for the high spatial resolution imaging of real biological samples, HeLa cells and rat brain tissue were analyzed and imaged using 70 keV $(CO_2)_{12000}$ and the data compared with that obtained using 70 keV $(H_2O)_{28000}$. Full details of sample preparation and the analytical protocols used are provided in the Supporting Information.

RESULTS AND DISCUSSION

Our results are reported in two sections. First, we report an investigation of the spectral and ion yield data obtained from the four biorelated molecules: trehalose, angiotensin, the sodium salt of a cardiolipin, and the phosopholipid, POPC. The purpose is to assess the benefits of water cluster beams compared to analogous argon and CO_2 based cluster beams in delivering ion yield across a variety of chemical types. As explained above the primary ion beam energy region below E/nucleon ~0.3 has been studied. Figure 1 shows two spectra from trehalose using 70 keV water and CO_2 cluster beams,

DOI: 10.1021/acs.analchem.9b01390
Anal. Chem. 2019, 91, 9058−9068

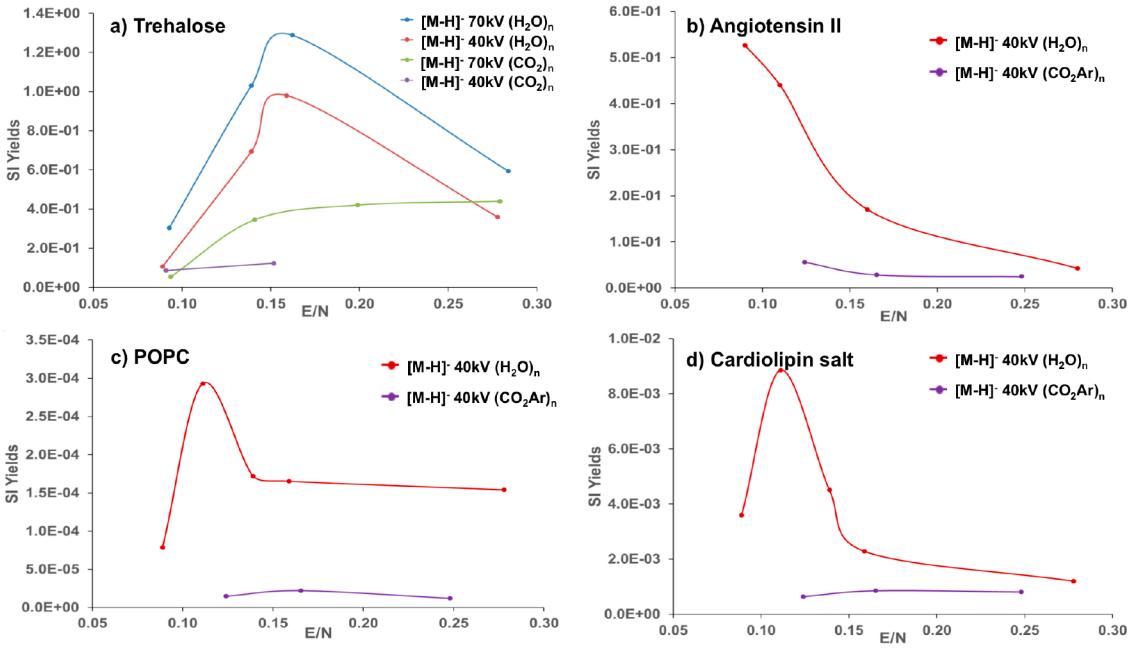

Figure 2. Variation of negative "molecular" secondary ion yields as a function of E/nucleon from (a) trehalose, comparing 40 and 70 keV $(CO_2)_n$ and $(H_2O)_n$ beams with a dose of 2×10^{12} ions cm^{-2}; (b) [Asn^1 Val^5] angiotensin II, comparing 40 keV $(ArCO_2)_n$ and $(H_2O)_n$ beams with an ion dose of 2×10^{12} ions cm^{-2}; (c) POPC comparing 40 keV $(ArCO_2)_n$ and $(H_2O)_n$ beams with an ion dose of 2×10^{12} ions cm^{-2} and (d) 1,1′,2,2′-tetraoleoyl cardiolipin (sodium salt) comparing 40 keV $(ArCO_2)_n$ and $(H_2O)_n$ beams with an ion dose of 5×10^{11} ions cm^{-2}.

where E/nucleon ~0.09. The major difference from our previous studies is that we immediately see enhancement not only of the positive ion yields but also *negative* ion yield compared to the (CO_2) cluster beam. Previously for instrumental reasons, negative ion detection was not available.[30,31] However, perhaps naively, we did not expect negative ion enhancement having focused on the possibility of enhanced proton attachment to molecules. Just by comparing the spectra, it can be seen that negative ion enhancement for molecularly related ions is as great if not greater than that for positive ions. The appearance of $(nM \pm H)$ ions as far as n = 10 or 12 is remarkable. This seems to support the idea that with these water cluster beams the emission region must be some sort of activated aqueous environment, where addition and loss of protons is possible involving quite large clusters of analyte molecules.

The spectra from trehalose obtained using water cluster beams at a given E/nucleon from each of the samples were qualitatively very similar using beam energies of 40 and 70 keV. The only difference was that the yields at 70 keV were higher than at 40 keV. The spectra obtained using argon or CO_2 cluster beams yields similar ions to those from the water beams but at much lower yield. The studies in Newcastle used pure argon or argon/CO_2 cluster beams, whereas at Penn State pure CO_2 cluster beams were used. Qualitatively the spectra using these three cluster beams did not differ. Some small differences in yields were noted but were not investigated systematically.

The comparative spectra using 40 keV water cluster beams and argon cluster beams at E/nucleon ~0.1 from the angiotensin, POPC and the cardiolipin are shown in Supporting Information, Figure S1. Again, clear positive and negative spectra are obtained with significant increases in yield using the water beams. The multimolecular peaks seen in the case of trehalose are not so much in evidence for these other compounds. Angiotensin shows a very considerable increase in $(M \pm H)$ and $(2M \pm H)$ peaks. The POPC sample had a significant salt content, so under the water beam in addition to increased yields of $(M \pm H)$ and $(2M \pm H)$, there are also increased yields of $(nM + Na)^+$ and $(nM + Cl)^-$ that mirror observations in our previous paper that the interactions with Na^+ are facilitated in the aqueous environment of the emission zone. The cardiolipin sample is a sodium salt so again not only are there increases in $M \pm H$ yields, there is also an increase in the $(M - Na)^-$ yield as the main negative ion. To test the capability of the water beam further, although not directly relevant as a side study, we investigated briefly its ability to generate the molecular ion of Insulin. Supporting Information, Figure S2 compares the spectra obtained from the oxidized B chain using 40 keV $(H_2O)_{16k}$ with $(CO_2)_{6k}$. It can be seen that the water beam delivers a strong $(M - NH)^-$ ion, where the signal is 20 times lower using the CO_2 beam.

Parts a–d of Figure 2 show the variation in ion yield for the principal negative "molecular" ions for the four compounds as a function of E/nucleon in the range below 0.3 (the positive ion plots are shown in Supporting Information, Figure S3). It can be seen that at E/nucleon close to 0.3, other than for POPC, the yields under the water beams and argon or CO_2 beams are roughly the same, supporting our previous conclusion that at this beam energy water beams in most cases behave in a similar fashion to argon or CO_2 beams. As we observed previously, using a cluster beam energy of 20 keV as E/nucleon falls the yields of the $M \pm H$ ions increase quite significantly and maximize in the region E/nucleon = 0.17 for trehalose (for both 40 and 70 keV beams) and 0.1 for POPC and cardolipin in agreement with our previous study.[30] Angiotensin is somewhat different in that that the ion yield is still increasing at the highest cluster size (or lowest E/nucleon) attainable. Significantly the insulin $(M - NH)^-$ ion also maximizes in this region (Supporting Information, Figure S2). As we concluded previously, there is something special

DOI: 10.1021/acs.analchem.9b01390
Anal. Chem. 2019, 91, 9058–9068

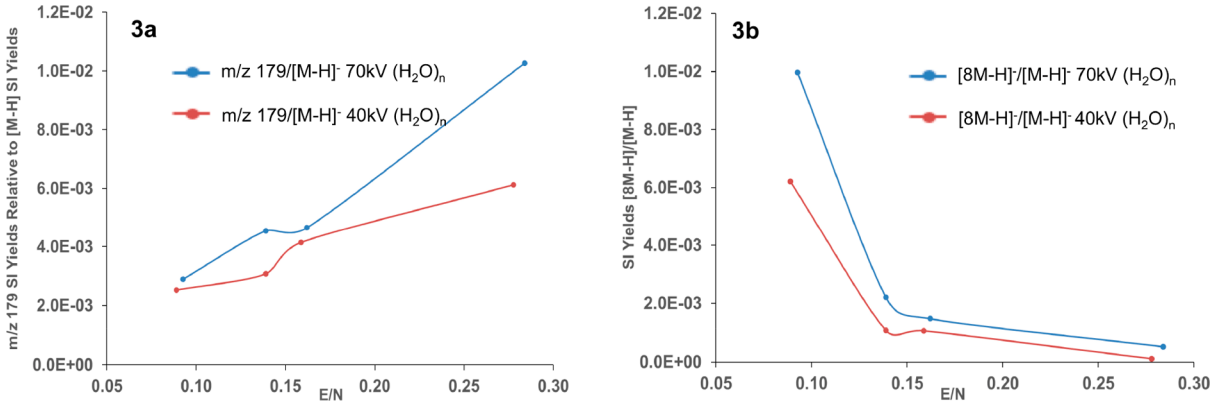

Figure 3. (a) Plot of the ratio of significant fragment m/z 179 ion yield relative to $(M - H)^-$ ion yield and (b) a plot of the ratio of ion yields of $(8M - H)^-/(M - H)^-$ yields from a trehalose film as a function of E/nucleon for the 40 and 70 keV $(H_2O)_n$ beams.

about the emission environment in this E/nucleon region that benefits ionization that involves proton attachment and detachment.[30,31] Some sort of activated aqueous zone seems most likely. However, while in all cases there is a significant yield enhancement under the water beam, the actual maximum ion yields from each pure compound still vary to a considerable degree from 1×10^{0} for trehalose, 5×10^{-1} for angiotensin, and 1×10^{-2} for the cardiolipin to 3×10^{-4} for POPC. Chemical effects continue to be important in determining the formation of ions.

In addition, in this cluster-beam energy region, as Figure 3a demonstrates, the yield of fragments also falls quite dramatically as the molecular peak is increasing. Again, this supports a somewhat gentler environment that encourages ionization and inhibits fragmentation. For trehalose, in contrast with the other compounds, the maximum in molecular ion yields occurs at E/nucleon close to 0.15 rather than ~0.1. However, as the M ± H yield falls beyond E/nucleon 0.15, there is a rapid increase in the formation of multimolecular ions $(nM - H)^-$ (see Figure 1) as plotted in Figure 3b that no doubt drains the M ± H emission channel. Clearly the trehalose molecules can interact and associate to form clusters that emit as stable ions. This observation provides further support for the concept of an aqueous like emission zone.

At low E/n, it was suggested previously that a concerted mechanism comes into play in which, because of their hydrogen-bonded stability, large water clusters largely retain their cluster geometry and interact with analyte molecules in the impact zone. There is sufficient activation energy generated by the impact to enhance protonation, but with minimal molecular fragmentation. In our earlier work using deuteration experiments to check the origin of protons involved in ion yield enhancement, we observed that both the ion yields and the extent of deuteration maximize at a beam energy in the region of 0.2 eV/nucleon.[30] MD simulations have shown that it is highly likely that at these low energies, the impacting cluster maintains a good deal of its structure.[43−45] Delcorte et al. have also studied the sputter yield and fragmentation of molecular species as a function of E/nucleon from large cluster impacts.[41,46] When E/nucleon falls significantly *below* 1 eV, the rate at which energy is deposited in the substrate is significantly slower. These authors showed that at E/nucleon ~0.2 eV, the time for the projectile to move 2 nm increases from about 100 fs to more than 300 fs. Thus, Delcorte's ideas suggest that impacting cluster particles are largely retained in the impact site over many 100s of fs and the molecules are moving more slowly, providing time for protonation (or deprotonation) to occur as the molecules are emitted from the surface.

The enhancement in yield over that observed using the argon or CO_2 beams varies between the compounds studied as is shown in Figure 4a,b. In these figures, we have presented a comparison of the maximum positive and negative ion signal generated from a 1 μm^2 area of the compound using the two beams. This is to enable us to discuss the benefits of water beams for bioimaging a little later.

It can be seen that the yield enhancement for trehalose $(M + H)^+$ is close to 100 times, whereas for the other molecules the $(M + H)^+$ enhancement ranges from around 5−13 to infinity for the cardiolipin. The case of angiotensin is interesting. The enhancement of $(M + H)^+$ is only 13, but the signal level is 6 times that of the trehalose $(M + H)^+$ ion and the angiotensin $(2M + H)^+$ enhancement is over 100×. If as we suggest the emission zone has some aqueous character, the way in which these molecules interact with water would be expected to play a role in the degree to which water enhances their ionization. Trehalose is a disaccharide with four exchangeable hydrogens per sugar ring, three on the ring OH groups and one CH_2OH group. The molecule can interact strongly with water and proton ionization must occur at one of these OH groups. The solubility of trehalose in water is high at ~70 mg/mL. Angiotensin has several amino groups that can also hydrogen bond with water, and its solubility is 25 mg/mL (https://www.chemicalbook.com). POPC has no exchangeable hydrogens and has a very low solubility. The cardiolipin we studied is in the form of a sodium salt and its solubility is also very low, however, its structure suggests the possibility of some interaction with OH groups and the possibility of sodium involvement. The range of ion signals and positive ion enhancements in Figure 4a seems to reflect in some way the degree to which the molecules interact with water, but it clearly not straightforward.

Figure 4b shows a rather different range of enhancements for the negative ions. The fact that negative ion enhancement occurs suggests that in the aqueous environment there is time for OH^- resulting from water autoionization to abstract hydrogens from the analyte molecules. While in contrast to the positive ion results, the enhancement of yields for trehalose are in the ×2−4 range; for angiotensin $(M - H)^-$, POPC $(M - H)^-$, and the cardiolipin $(M - Na)^-$ results in enhancements of ×10 to over ×20. This is further evidence that some sort of dynamic chemical interaction must occur in the aqueous

DOI: 10.1021/acs.analchem.9b01390
Anal. Chem. 2019, 91, 9058−9068

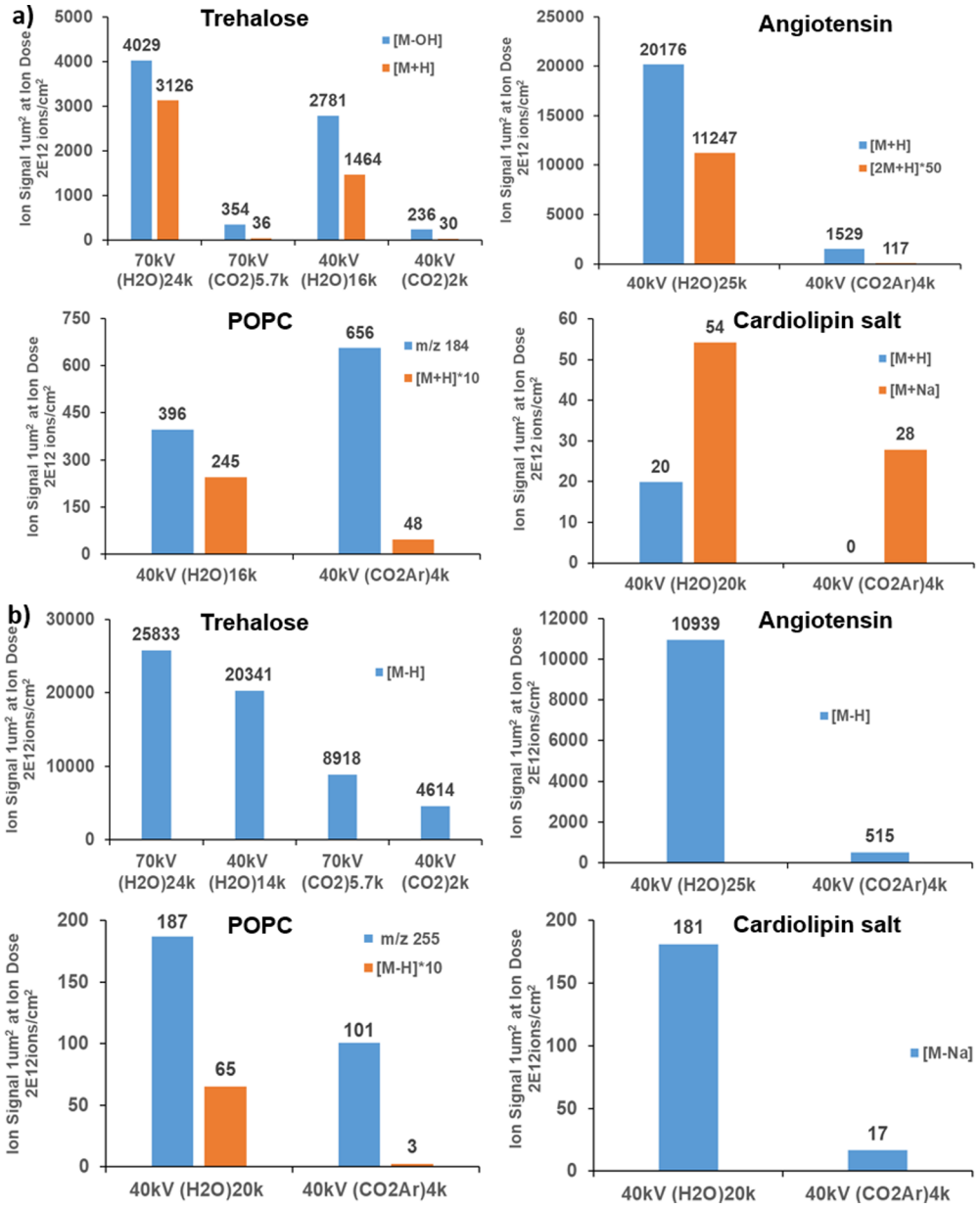

Figure 4. (a) Maximum positive SI yields of trehalose, angiotensin, and POPC from 1 μm^2 area acquired after steady state with an ion dose of 2×10^{12} ions cm^{-2}, and cardiolipin salt acquired at ion dose of 5×10^{11} ions cm^{-2} at layer 3 using 40 keV H_2O cluster beam compared to yields obtained using 40 keV $(CO_2)_{4k}$. (b) Maximum negative SI Yields of trehalose, angiotensinm and POPC from 1 μm^2 area acquired after steady state with an ion dose of 2×10^{12} ions cm^{-2}, and Cardiolipin acquired at ion dose of 5×10^{11} ions cm^{-2} at layer 3 compared to yields obtained using 40 keV $(CO_2)_{4k}$.

emission zone. There is sufficient energy and a water environment to promote the protonation, hydrogen abstraction, and Na abstraction as the molecules move through the emission zone to exit the surface. For trehalose, the dynamic equilibrium is obviously well over to the protonation side, so negative ion enhancement is less than the many positive ions observed. The oxidation of POPC by active OH is a known reaction, hence the enhancement of $(M - H)^-$ and $(2M - H)^-$ is understandable.[29] Similarly the dimer of angiotensin seems to enter a dynamic state in water to yield both $(2\ M \pm H)^{\pm}$ in high yield. In the aqueous environment, the formation of negative cardiolipin ions by loss of Na^+ to water is enhanced.

Of course, an increase in ionization probability in the aqueous emission zone is reflected in these enhancements. If Wucher's estimate of 10^{-3} for the ionization probability of a compound such as trehalose under C_{60} or argon cluster bombardment is correct, and because we are seeing a factor of ×10 to ×100 increase in positive ion yields under water beams compared to CO_2 cluster beams for $(M - OH)^+$ and $(M + H)^+$, this might imply ionization probability levels of up to a few percent, which would be a remarkable increase.

We cannot easily measure ionization probabilities, but we can estimate *Useful Yields* (UYs, detected "molecular" ion yield/number of molecules sputtered). The number of detected molecular ions will be dependent on the ionization probability, the survival probability, and the efficiency of the ToF-SIMS ion transmission and detection system. As noted in the Supporting Information, the analogue detection system of the J105 amplifies the detection of one ion to yield a signal level of 60−70. While the enhanced signal is mainly beneficial,

DOI: 10.1021/acs.analchem.9b01390
Anal. Chem. 2019, 91, 9058−9068

Table 1. Comparison of Estimated Useful Yields per Ion Impact for the Cluster Beams Used for the Analysis of Trehalose[a]

	C_{60} (40 keV)	Ar_n (20 keV)	Ar_n + HCl (20 keV)	$(CO_2)_{6k}$ 40 keV E/nucl ~0.16	$(H_2O)_{7k}$ 20 kV E/nucl ~0.16	$(H_2O)_{14k}$ 40 keV E/nucl ~0.16	$(H_2O)_{24k}$ 70 keV E/nucl ~0.16	$(H_2O)_{42k}$ 70 keV E/nucl ~0.09
sputter yield				116 nm^3	55 nm^3	111 nm^3	190 nm^3	160 nm^3
$(M - OH)^+$	2×10^{-6}	2×10^{-6}	2×10^{-6}	4×10^{-7}	6×10^{-6}	7.5×10^{-6}	5.5×10^{-6}	2.2×10^{-6}
$(M + H)^+$	5×10^{-8}	8×10^{-8}	2×10^{-6}	5×10^{-8}	6×10^{-6}	4×10^{-6}	4×10^{-6}	1.2×10^{-6}
$(M - OH) + (M + H)$				4.5×10^{-7}	1.2×10^{-5}	1.2×10^{-5}	1×10^{-5}	3.5×10^{-6}
$(M - H)^-$	8×10^{-7}	4×10^{-6}	3×10^{-8}	6.5×10^{-6}	6.3×10^{-5}	5.5×10^{-5}	4.3×10^{-5}	8×10^{-6}

[a]The data in columns 1−3 from Wucher,[21] columns 5−8, this work.

to compare Useful Yields (UYs) with other ToF-SIMS instruments, we need to correct the J105 signal. Also, in this work, we have not directly measured sputter yields; instead, we use the Universal Sputtering plot reported in our first paper to obtain estimates of the sputter yield of the cluster beams used.[24] While comparing UYs between instrument configurations is of interest, our concern here is to use UYs to indirectly discern changes in ionization probability (combined with survival probability) as between different cluster beam configurations. All the data comes from a J105 instrument. Table 1 compares some of the UYs for trehalose reported in Wucher's paper with those obtained in this work. There are a number of interesting features to highlight in this data. The UY of the $(M + H)^+$ ion under argon or CO_2 cluster bombardment is constant in the high 10^{-8} independent of beam energy and cluster size. Using the water beam, the UY jumps almost 2 orders to $\sim 5 \times 10^{-6}$ or 10^{-5} for $(M + H)^+$, so because UY takes account of material sputtered and we are comparing data from J105 instruments, we conclude that the positive ionization probability in concert with the survival probability has increased for the production of positive molecular ions by almost two orders. The UYs for the negative ion $(M - H)^-$ behave similarly although the increase between the CO_2 and water cluster yields is only about 10.

It is difficult to model trends in the survival probability. For trehalose, there are two pathways for the loss of $(M - H)^-$ ions, one via molecular ion fragmentation, which decreases as E/nucleon falls, and the other by the formation of multimolecular ions whose yield increases as shown in Figure 3. In the final three columns of Table 1, we present the UYs for 70 keV water beams using clusters sizes where E/nucleon decreases from 0.16 to 0.09. The UYs decrease from 4.3×10^{-5} to 8×10^{-6}, which seems to correlate with the multimolecular ion yield increase to E/nucleon 0.09. If we include the multimolecular ion yield up to $(12M - H)^-$ into the UY calculation, the UY is restored to 2×10^{-5}, not too far below that obtained at E/nucleon 0.16, suggesting that the ionization probability to $(M - H)^-$ remains constant, but the survival probability is declining due to loss of ions to multimolecular ion formation.

In our previous study, at 20 keV, the optimum yield was observed with a cluster size around 6000−7000 water molecules.[30] We speculated that if the cluster size could be increased by increasing the beam energy further at the optimum E/nucleon, further increases in ion yield might result. Supporting Information, Figure S4 confirms this hypothesis. The ion yield for the positive and negative ion yields from trehalose increase by a factor around 3 between 20 and 70 keV beams for E/nucleon of 0.16. The water cluster size increased from 6000 to 24000 molecules. The question arises as to whether this increase in yield as a function of beam energy is a result of a further increase in ionization probability or to generating more analyte molecules in the emission zone.

We see from Table 1 that at constant E/nucleon (~0.16) for the water beams, the UY for both positive and negative ions is almost constant with beam energy and cluster size. The sputter yield/nucleon will be constant, but the sputter yield per cluster increases in line with cluster size, so a constant UY implies that the ionization probability remains constant. Thus we conclude that the main benefit of increased beam energy at the optimum E/nucleon is an increase in sputtered material that is then ionized at a constant rate. Table 1 shows that the sputter yield increases by about ×3.5 between 20 keV $(H_2O)_{6.5k}$ and 70 keV $(H_2O)_{25k}$, which is very similar to the rise in ion yield shown in Supporting Information, Figure S4, over this cluster beam range. Thus, in this emission regime, the ionization probability for a given molecule seems to be constant at constant E/nucleon and independent of cluster size.

Of course, trehalose and angiotensin show the greatest yields, while POPC and cardiolipin show several orders less sensitivity even under the water beam. This might imply significantly lower ionization probabilities, which would accord with the fact that they lack easily exchangable hydrogens,[22] although the absolute values cannot be inferred without knowing more about the degree to which the molecular ion fragments. However, although the estimated UY for the POPC negative $(M - H)^-$ ion is only 1.8×10^{-8} under the water beam, this is still 30 times greater than under the CO_2 cluster beam. As we shall see, this is sufficient to deliver good yields of lipid ions in cell and tissue imaging.

Does the water beam advance our aim to increase ion yields in order to increase the feasibility of submicrometer analysis and imaging? We asked this question in our first paper that only dealt with positive ions. We saw that the answer was: broadly yes. Combining the yield enhancements with the capability of the J105 to accumulate ions over a larger primary ion dose enabled detected positive molecular ion signals from a 1 μm^2 area to be increased by 10−100 times compared to yields using argon cluster ions under static conditions. The benefit of these enhancements were subsequently realized using water cluster beams to image rat brain, resulting in the detection of lipids and other molecules that had been difficult to detect previously.[40]

The present work shows that these benefits are also accessible for negative molecular ions. Parts a and b of Figure 4 display the positive and negative ion signals measured from a 1 μm^2 area using a ion beam dose of 2×10^{12} cm^{-2}, respectively, an ion beam dose close to that used for imaging purposes. It can be seen that while yields from trehalose and angiotensin are very high such that these compounds would be detectable in sub-1% concentrations, even compounds such as POPC and the cardiolipin that are very hard to ionize with

DOI: 10.1021/acs.analchem.9b01390
Anal. Chem. 2019, 91, 9058−9068

argon or CO_2 cluster beams become detectable at the few % level with the water beam. Collecting ions at higher dose levels, as is eminently possible using the J105 configuration, e.g., 1×10^{13} will enable this limit to be pushed below 1%. As we demonstrate in the next section, water beams greatly enhance the bioimaging capability of ToF-SIMS.

CELL AND TISSUE ANALYSIS AND IMAGING

The study on the standards analysis has confirmed that the water cluster ion beam enhances the molecular ion, protonated or deprotonated, many-fold. In the following, we cross compare H_2O and CO_2 cluster beams on real biological samples to investigate the degree to which the enhancement is observed in complex biomatrices and to evaluate the potential contribution of the high energy water cluster beam to high resolution imaging.

In Supporting Information, Figure S5, the normalized spectra (averaged to pixels of cellular region and beam current) directly compare the intact lipids in the range of m/z 600−1550 using 70 keV $(CO_2)_{13.9k}$ and $(H_2O)_{29k}$ beams (both E/nucleon ~0.13) on air-dried cells and on cryofixed frozen-hydrated cells. It clearly shows that the lipid signals are increased dramatically using the water beam, especially for cardiolipin (CL) in the frozen-hydrated cell. Presumably, the sample preparation is also contributing to signal enhancement due to the better preservation of chemistry using cryofixation, although cryofixation does not seem to enhance the spectral yield using the CO_2 cluster beam (Supporting Information, Figure S5b). The enhancement due to the use of the water beam is further highlighted by comparing the yields from selected lipids species shown in Table 2. In line with our expectations from the standards work, at least 1 order of magnitude increase is seen for intact phospholipids (PL) and cardiolipins (CL) from the air-dried sample compared with the CO_2 beam, and further enhancement up to 121 times for intact PL and 500 times for CLs is observed using the water beam on frozen-hydrated cells. There are a few ions where the enhancement is not so great, e.g., those observed at m/z 835.50, 863.53, and 885.51, where only a 3−4 times of increase is seen on frozen-hydrated cells. This indicates that the chemical fixation could lift these lipids to the membrane surface for detection. In contrast, cryofixation has preserved most pristine chemistry on the cell membrane, especially for the water solution lipids like phosphatidic acid (PA) at m/z 773.52 and phosphatidylserine (PS) at m/z 760.53, which are likely to diffuse away during glutaraldehyde fixation. Moreover, more CL species at m/z 1441.93, 1455.97, 1467.96, and 1495.98 are dramatically enhanced in the frozen-hydrated cells using water cluster beam, while there is little or no enhancement on these cells using CO_2 cluster beam, indicating that both water cluster and sample preparation play important role in ionization improvement. The major fatty acid fragments are only enhanced by 3−5 times, much less than for intact lipids, reflecting lower fragmentation expected using the water beam.

For the cell imaging, the $(H_2O)_{28k}^+$ was focused down to 1 μm after calibrating on a 1000 mesh SEM grid. To preserve the pristine chemistry, the cells were kept frozen-hydrated and analyzed at 100 K. The total ion and selected ion overlay images from selected depths are shown in Figure 5A. The complete depth profile is show in Figure S6. The cells are consumed away gradually by the water beam, as shown in the total ion images. The yield enhancement for intact lipids now

Table 2. Negative Ion Signal Yields from Cell Lipids As a Function of Analysis Conditions, Presented as a Ratio Compared to the Yields Obtained Using a CO_2 Cluster Beam on a Chemically Fixed Sample at Room Temperature[a]

m/z	H_2O beam cryofixed	CO_2 beam cryofixed	H_2O chem fixed RT	CO_2 chem fixed RT
		Fatty Acids		
255.21	4.91	0.36	4.09	1
281.22	3.93	0.28	3.59	1
283.24	3	0.66	5.37	1
		Intact Lipids		
673.4	12.24	0.93	11.08	1
687.51	14.88	0.72	14.9	1
701.49	15.34	1.26	19.1	1
747.53	26	1.22	11.31	1
760.53	28.34	4.02	13.19	1
773.52	**40.73**	0.79	15.95	1
788.53	28.33	3.02	17.58	1
810.53	18.33	0.73	22.01	1
835.49	3.23	0.27	15.46	1
847.42	**121.11**	0.77	14.64	1
863.53	3.92	0.29	18.21	1
873.44	**34.89**	2.4	5.75	1
885.56	3.19	0.45	24.11	1
		Cardiolipins		
1403.99	**60.14**	2.32	13.73	1
1430.03	**118.56**	0.67	13.88	1
1441.93	**108.52**	5.5	18.08	1
1455.97	**418.94**	0.65	29.64	1
1467.96	**509.42**	3.26	12.49	1
1495.98	**161**	4.71	32.05	1

[a]Bold data highlight a very significant enhancement of yield.

enables us to use phosphatidylglycerol, PG (34:1), PS (36:1), and phosphatidylinositol, PI (38:4), at m/z 747.50, 788.50, and 885.52 to map cellular membrane directly (green), deprotonated CLs to map the mitochondria membrane (magenta), and the sugar−phosphate backbone at m/z 195.02 to map the nuclei (blue) in the color overlay images, respectively. The same batch of sample was also analyzed using $(CO_2)_{12k}^+$, as shown in Figure 5B. Interestingly, CLs are clearly localized in the perinuclear region at depth of L1-L7 by using the water beam due to the ionization enhancement particularly for larger CLs molecules, while their distribution is not clear after profiling through the first two layers using the CO_2 beam as in Figure 5B. A reconstruction of a depth profile of HeLa cells after z-correction is shown in the movie in Supporting Information, Figure S7.[47] It is displayed as horizontal slices of the cells: the cell membrane in green, the distribution of CLs reflecting the mitochondria in red between the membrane in green, and the nucleus shown in blue. It is also very interesting to be able to distinguish the distributions of different PLs on the cell membrane as in Figure 6a, PG (34:1) in green, PS(36:1) in magenta, and PI(38:4) in cyan that are evident in the first layer of depth profiling of the frozen-hydrated cells. On a single cell as the arrow indicates, PS is generally toward to the edge of the cellular membrane, PI is more centralized. The ion intensities of m/z 747.50 and 885.52 have been monitored across the nucleus highlighted by a white square in Figure 6b. The yield of the ion at m/z 747.50 is higher further away from the nucleus while that at m/z 885.52 is more

DOI: 10.1021/acs.analchem.9b01390
Anal. Chem. 2019, 91, 9058−9068

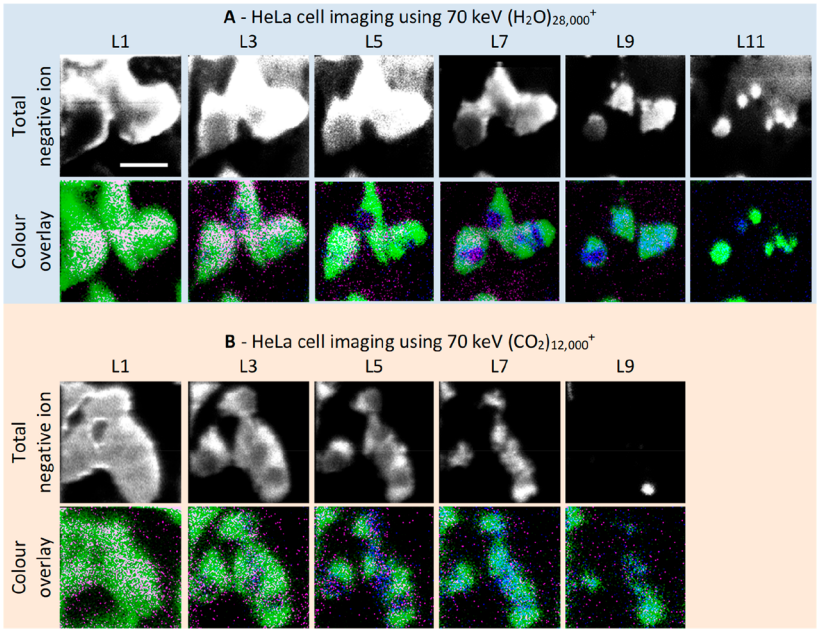

Figure 5. Total ion and color overlay image from selected depths of HeLa cells undergoing depth profiling using 70 keV $(H_2O)_{28k}^+$ in (A) and 70 keV $(CO_2)_{12k}^+$ in (B). Scale bar is 50 μm. The sequence of images were acquired with 128 × 128 pixel over 128 × 128 μm^2 with an ion dose of 9.3 × 10^{12} ions/cm^2 using H_2O cluster beam and 1.9 × 10^{13} ions cm^{-2} using CO_2 cluster beam for each layer. L1 denotes layer 1, L5 layer 5, etc. The total negative ion images are shown as gray scale image. The color overlay images show the distribution of different biospecies. Green: PG (34:1), PS(36:1), and PI(38:4) at m/z 747.50, 788.50, and 885.52. Magenta: cardiolipins CL(68:2), CL(70:3), CL(72:11), and CL(72:4) at m/z 1403.99, 1430.02, 1441.93, and 1456.03. Blue: Phosphate−sugar backbone at m/z 195.02.

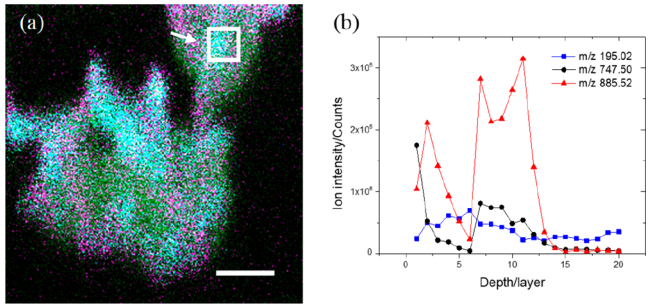

Figure 6. Color overlay image of selected lipid molecular ions on the frozen-hydrated HeLa cell membrane in (a). Scale bar is 50 μm. Green: PG (34:1) at m/z 747.50. Magenta: PS(36:1) at m/z 788.50. Cyan: PI(38:4) at m/z 885.52. Scale bar is 50 μm. (b) Ion intensity of m/z 195.02 (blue points), m/z 747.50 (black points), and m/z 885.52 (red points) in the highlighted area that includes the nucleus are plotted as a function of the depth. It indicates that m/z 747.50 assigned to PG (34:1) is in the outer layer of the membrane, while the m/z 885.52 as PI(38:4) is in the inner leaflet of the membrane. m/z 195.02 as phosphate−sugar backbone of the nucleic acid reaches the maximum where the lipids are absent (around layer 6).

intense close to nucleus as shown in m/z 195.02 (sugar phosphate backbone of nucleic acids). This indicates that m/z 747.50 assigned to PG (34:1) is in the outer layer of the membrane, while m/z 885.52 as PI(38:4) is concentrated in the inner leaflet of the membrane. To our knowledge, this is the first time the CLs and different PLs have been mapped at single cell level, attributing to the favorable ionization of larger intact lipids using water cluster beam.

Negative ion signal enhancement using H_2O cluster beam has also been verified on rat brain tissue. From the cornu ammonis CA3 region (blue square area in Figure 7a on two consecutive rat brain tissues, the use of 70 keV $(H_2O)_{34k}^+$ results in up to 15 times greater single yield from intact lipids signal compared with 70 keV $(CO_2)_{13.9k}^+$, as shown in Supporting Information, Table S1. This is especially evident for the low concentration lipids such as phosphatidylethanolamine (PE), where the signal enhancement facilitates the localization of these lipids on the biological sample. As shown in Figure 7b, the yield of PE(36:4) is enhanced 10.8-fold using H_2O cluster beam (Supporting Information, Table S1), and its localization (yellow) is clearly seen in a narrow layer of the inner CA3 region, the stratum lucidum. In contrast, the localization of this ion is not seen using the CO_2 cluster beam (Figure 7c) at the same ion dose. With the higher dose of the CO_2 beam, PE has been mapped in CA3 region in previous work.[10] With five times enhancement using the water cluster beam, PI (38:6) is clearly shown in the pyramidal layer as mapped in cyan (Figure 7b). The CA3 region plays an important role in memory processes, seizure susceptibility, and neurodegeneration. To understand the biochemistry changes in the region would provide new insight of molecular mechanism in health and diseased state. Imaging with water cluster beam is a leap toward the understanding the biochemistry at cellular level owing to the higher chemical sensitivity and high spatial resolution which matches anatomical features.

A larger area of dentate gyrus (DG) (green box area in Figure 7a was also imaged using water cluster beam as in Figures 7d,e. Five distinct cellular biomolecules were distinguished with in bands of 50−100 μm width. It is intriguing that gangliosides GM1 (36:1) in m/z 1544.86 in **green** and GM1 (38:1) at m/z 1572.91 in **magenta** are located next to each other in the middle, while sulfatide ST (18:0) at m/z 806.5 in **yellow** and PI (38:4) at m/z 885.56 in **blue** are located on either side (Figure 7e). The DG area is one of few brain structures related to adult neurogenesis in many mammal

DOI: 10.1021/acs.analchem.9b01390
Anal. Chem. 2019, 91, 9058−9068

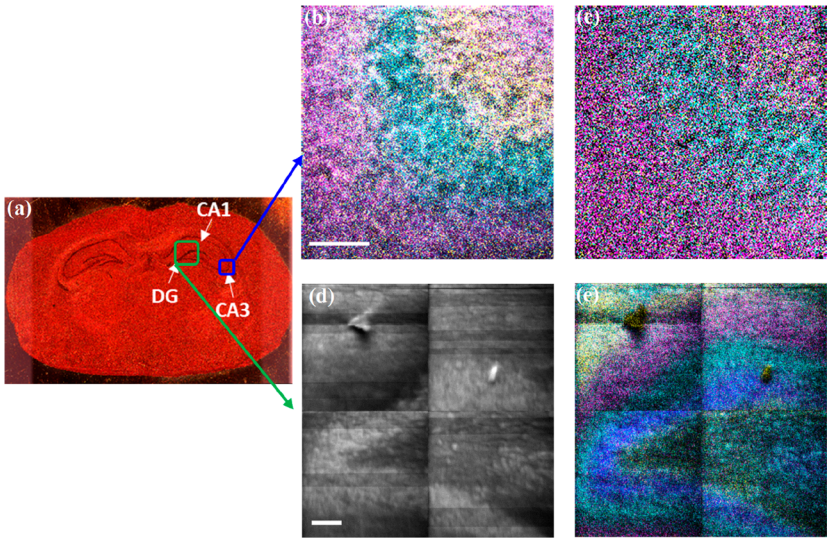

Figure 7. Cluster beam imaging of **cornu ammonis (CA3)** and **dentate gyrus (DG)** region. (a) H&E staining image of consecutive section. CA3 and DG region are shown in blue and green square. **For CA3 region**: color overlay images of consecutive rat brain tissues using (b) 70 keV $(H_2O)_{34k}^+$ and (c) $(CO_2)_{13.9k}^+$. Yellow: PE (36:4) at m/z 722.52. Blue: PI (38:5) at m/z 883.56. Magenta: PS (40:6) at m/z 834.56. The images were acquired with 256 × 256 pixels over 420 × 420 μm^2 with an ion dose of 1.2 × 10^{13} ions cm^{-2} for both beams. Because of the ionization enhancement of 10.8-fold, PE 36:4p (yellow) is clearly shown in a narrow layer, the stratum lucidum using H_2O beam. In contrast, the localization of this ion is not seen using CO_2 beam. **For DG region**: total negative ion image using 70 keV $(H_2O)_{34k}^+$ (d) and color overlay image (e). Yellow: sulfatide ST (18:0) at m/z 806.58. Blue: PI (38:4) at m/z 885.56. Green: ganglioside GM1 (36:1) at m/z 1544.86. Magenta: GM1 (38:1) at m/z 1572.91. The images were acquired using 2 × 2 tiles. Each tile contains 256 × 256 pixel over 420 × 420 μm^2 with an ion dose of 1.2 × 10^{13} ions cm^{-2}. Scale bar is 100 μm and image pixel size is about 1.5 μm.

species include human.[48] With richer chemical information and comparable spatial resolution as traditional staining/fluorescence image, SIMS image likely provides the further understanding of biofunction of neurogenesis in this region.

CONCLUSIONS

1. As previously, we show that above E/nucleon ∼0.3 water and nonwater containing cluster beams generate very similar ion yields, as E/nucleon is reduced under the water beams yields of BOTH negative and positive "molecular" ions increase significantly, in many cases maximizing in the E/nucleon <0.16 region with yield increases of ∼10−100.
2. Ion fragment yields in general decrease quite dramatically in this region.
3. At a constant E/nucleon in region below ∼0.2, secondary ion yield increases with beam energy and hence cluster size. By estimating Useful Yields, it is shown that the ionization probability is broadly constant at constant E/nucleon, the yield increase is due to increased sputtering yield.
4. The model of an emission zone with aqueous character seems to be sustained.
5. Cell and tissue imaging using a focused H_2O cluster beam has been demonstrated at the 1 μm level, and the very significant ionization enhancements available using the water beams are applicable to real and complex biomatrices. This will eventually benefit high spatial resolution imaging of many lipid species, especially those encountered at low concentrations. The developments reported here serve as a further stepping stone to enabling our understanding of the arrangement and asymmetry of cellular membrane lipids that should enhance our insights into the molecular mechanism of lipid related signaling and function.

ASSOCIATED CONTENT

Supporting Information

This material is available free of charge at https//pubs/acs/org. The Supporting Information is available free of charge on the ACS Publications website at DOI: 10.1021/acs.analchem.9b01390.

Sample preparation, analytical methods, cell and tissue imaging details, and supplementary figures (PDF)

Depth profile of a HeLa cell (AVI)

AUTHOR INFORMATION

Corresponding Author

*E-mail: hut3@psu.edu.

ORCID

Hua Tian: 0000-0002-3598-0219

Present Addresses

S.S. Photon Science Institute, University of Manchester, Manchester, United Kingdom

P.C. Mark Wainwright Analytical Centre, University of New South Wales, Sydney, Australia

J.C.V. is an Emeritus Professor at the University of Manchester. During this work, he was an honorary visiting Professor at the University of Newcastle.

Author Contributions

S.S. and H.T. contributed equally to the experimental studies. They and J.C.V. produced the manuscript.

Notes

The authors declare no competing financial interest.

DOI: 10.1021/acs.analchem.9b01390
Anal. Chem. 2019, 91, 9058−9068

■ ACKNOWLEDGMENTS

We thank James Hood and Michael Foster for assistance with maintenance of ToF-SIMS and Professor Ian W. Fletcher for general advice and assistance in the Newcastle ToF-SIMS laboratory. The ToF-SIMS instrument at Newcastle University was purchased, in part, under an instrument package funded by EPSRC capital funding grant EP/K022679/1. The work at Pennsylvania State University was supported by NIH grants 5R01GM113746-21 and U54GM103529-08. The tissue samples were generously provided by Prof. Valerian E. Kagan, Prof. Hulya Bayir and Dr. Louis J. Sparvero in University of Pittsburgh. We thank Dr. Dan Graham and Dr. Sebastiaan Van Nuffel for the help with *z*-correction of HeLa cell 3D imaging.

■ REFERENCES

(1) Boxer, S. G.; Kraft, M. L.; Weber, P. K. *Annu. Rev. Biophys.* **2009**, *38*, 53−74.
(2) Fletcher, J. S.; Vickerman, J. C.; Winograd, N. *Curr. Opin. Chem. Biol.* **2011**, *15*, 733−740.
(3) Gamble, L. J.; Anderton, C. R. *Microsc. Today* **2016**, *24*, 24−31.
(4) Pól, J.; Strohalm, M.; Havlíček, V.; Volný, M. *Histochem. Cell Biol.* **2010**, *134*, 423−443.
(5) Passarelli, M. K.; Winograd, N. *Biochim. Biophys. Acta, Mol. Cell Biol. Lipids* **2011**, *1811*, 976−990.
(6) Vickerman, J. C. *Analyst* **2011**, *136*, 2199−2217.
(7) Rabbani, S.; Barber, A. M.; Fletcher, J. S.; Lockyer, N. P.; Vickerman, J. C. *Anal. Chem.* **2011**, *83*, 3793−3800.
(8) Toyoda, N.; Matsuo, J.; Aoki, T.; Yamada, I.; Fenner, D. B. *Nucl. Instrum. Methods Phys. Res., Sect. B* **2002**, *190*, 860−864.
(9) Mohammadi, A. S.; Phan, N. T. N.; Fletcher, J. S.; Ewing, A. G. *Anal. Bioanal. Chem.* **2016**, *408*, 6857−6868.
(10) Tian, H.; Sparvero, L. J.; Blenkinsopp, P.; Amoscato, A. A.; Watkins, S. C.; Bayir, H.; Kagan, V. E.; Winograd, N. *Angew. Chem.* **2019**, *131*, 3188−3193.
(11) Angerer, T. B.; Blenkinsopp, P.; Fletcher, J. S. *Int. J. Mass Spectrom.* **2015**, *377*, 591−598.
(12) Tian, H.; Sparvero, L. J.; Amoscato, A. A.; Bloom, A.; Bayir, H.; Kagan, V. E.; Winograd, N. *Anal. Chem.* **2017**, *89*, 4611−4619.
(13) Vickerman, J. C.; Winograd, N. *Int. J. Mass Spectrom.* **2015**, *377*, 568−579.
(14) Busch, K. L.; Hsu, B. H.; Xie, Y. X.; Cooks, R. G. *Anal. Chem.* **1983**, *55*, 1157−1160.
(15) Adriaens, A.; Ferauge, C.; Adams, F. *Int. J. Mass Spectrom. Ion Processes* **1995**, *151*, 63−68.
(16) Shard, A. G.; Spencer, S. J.; Smith, S. A.; Havelund, R.; Gilmore, I. S. *Int. J. Mass Spectrom.* **2015**, *377*, 599−609.
(17) Benninghoven, A. *Angew. Chem., Int. Ed. Engl.* **1994**, *33*, 1023−1043.
(18) Gillen, G.; Szakal, C.; Brewer, T. M. *Surf. Interface Anal.* **2011**, *43*, 376−379.
(19) Cheng, J.; Kozole, J.; Hengstebeck, R.; Winograd, N. *J. Am. Soc. Mass Spectrom.* **2007**, *18*, 406−412.
(20) Zhang, J.; Franzreb, K.; Aksyonov, S. A.; Williams, P. *Anal. Chem.* **2015**, *87*, 10779−10784.
(21) Wucher, A. *J. Vac. Sci. Technol., B: Nanotechnol. Microelectron.: Mater., Process., Meas., Phenom.* **2018**, *36*, 03F123.
(22) Breuer, L.; Tian, H.; Wucher, A.; Winograd, N. *J. Phys. Chem. C* **2019**, *123*, 565−574.
(23) Heeger, M.; Tyler, B. J.; Körsgen, M.; Arlinghaus, H. F. *Biointerphases* **2018**, *13*, 03B412.
(24) Adriaensen, L.; Vangaever, F.; Gijbels, R. *Anal. Chem.* **2004**, *76*, 6777−6785.
(25) Fitzgerald, J. J. D.; Kunnath, P.; Walker, A. V. *Anal. Chem.* **2010**, *82*, 4413−4419.
(26) Kim, Y.-P.; Oh, E.; Hong, M.-Y.; Lee, D.; Han, M.-K.; Shon, H. K.; Moon, D. W.; Kim, H.-S.; Lee, T. G. *Anal. Chem.* **2006**, *78*, 1913−1920.
(27) Sämfors, S.; Ewing, A. G.; Fletcher, J. S. *Rapid Commun. Mass Spectrom.* **2018**, *32*, 1473−1480.
(28) Wu, K. J.; Odom, R. W. *Anal. Chem.* **1996**, *68*, 873−882.
(29) Sheraz née Rabbani, S.; Barber, A.; Fletcher, J. S.; Lockyer, N. P.; Vickerman, J. C. *Anal. Chem.* **2013**, *85*, 5654−5658.
(30) Sheraz née Rabbani, S.; Berrueta Razo, I.; Kohn, T.; Lockyer, N. P.; Vickerman, J. C. *Anal. Chem.* **2015**, *87*, 2367−2374.
(31) Sheraz née Rabbani, S.; Barber, A.; Berrueta Razo, I.; Fletcher, J. S.; Lockyer, N. P.; Vickerman, J. C. *Surf. Interface Anal.* **2014**, *46*, 51−53.
(32) Conlan, X. A.; Lockyer, N. P.; Vickerman, J. C. *Rapid Commun. Mass Spectrom.* **2006**, *20*, 1327−1334.
(33) Mouhib, T.; Delcorte, A.; Poleunis, C.; Bertrand, P. *Surf. Interface Anal.* **2013**, *45*, 46−49.
(34) Roddy, T. P.; Cannon, D. M.; Ostrowski, S. G.; Ewing, A. G.; Winograd, N. *Anal. Chem.* **2003**, *75*, 4087−4094.
(35) Fletcher, J. S.; Rabbani, S.; Henderson, A.; Blenkinsopp, P.; Thompson, S. P.; Lockyer, N. P.; Vickerman, J. C. *Anal. Chem.* **2008**, *80*, 9058−9064.
(36) Tian, H.; Wucher, A.; Winograd, N. *Surf. Interface Anal.* **2014**, *46*, 115−117.
(37) Wucher, A.; Tian, H.; Winograd, N. *Rapid Commun. Mass Spectrom.* **2014**, *28*, 396−400.
(38) Tian, H.; Maciążek, D.; Postawa, Z.; Garrison, B. J.; Winograd, N. *J. Am. Soc. Mass Spectrom.* **2016**, *27*, 1476−1482.
(39) Alnajeebi, A. M.; Vickerman, J. C.; Lockyer, N. P. *Rapid Commun. Mass Spectrom.* **2018**, *32*, 1962−1970.
(40) Berrueta Razo, I.; Sheraz, S.; Henderson, A.; Lockyer, N. P.; Vickerman, J. C. *Rapid Commun. Mass Spectrom.* **2015**, *29*, 1851−1862.
(41) Delcorte, A.; Restrepo, O. A.; Czerwinski, B.; Garrison, B. J. *Surf. Interface Anal.* **2013**, *45*, 9−13.
(42) Edwards, R.; Mesfin, H. M.; Pospisilova, E.; Poleunis, C.; Bailly, C.; Delcorte, A. *J. Vac. Sci. Technol., B: Nanotechnol. Microelectron.: Mater., Process., Meas., Phenom.* **2018**, *36*, 03F118.
(43) Postawa, Z.; Paruch, R.; Rzeznik, L.; Garrison, B. J. *Surf. Interface Anal.* **2013**, *45*, 35−38.
(44) Seah, M. P.; Havelund, R.; Gilmore, I. S. *J. Phys. Chem. C* **2014**, *118*, 12862−12872.
(45) Mücksch, C.; Anders, C.; Gnaser, H.; Urbassek, H. M. *J. Phys. Chem. C* **2014**, *118*, 7962−7970.
(46) Delcorte, A.; Garrison, B. J.; Hamraoui, K. *Anal. Chem.* **2009**, *81*, 6676−6686.
(47) Robinson, M. A.; Graham, D. J.; Castner, D. G. *Anal. Chem.* **2012**, *84*, 4880−4885.
(48) Drew, L. J.; Fusi, S.; Hen, R. *Learn. Mem.* **2013**, *20*, 710−729.

DOI: 10.1021/acs.analchem.9b01390
Anal. Chem. 2019, 91, 9058−9068